Journal of Power Sources 196 (2011) 5599–5603

Contents lists available at ScienceDirect

Journal of Power Sources

journal homepage: www.elsevier.com/locate/jpowsour

Short communication

Mechanical properties of solid oxide fuel cell glass-ceramic seal at high temperatures

J. Milhans[a,*], D.S. Li[b], M. Khaleel[b], X. Sun[b], Marwan S. Al-Haik[c], Adrian Harris[d], H. Garmestani[a]

[a] School of Material Science and Engineering, Georgia Institute of Technology, Atlanta, GA 30332-0245, United States
[b] Fundamental and Computational Sciences Directorate, Pacific Northwest National Laboratory, Richland, WA 99354, United States
[c] Department of Engineering Science and Mechanics, Virginia Polytechnic Institute and State University, Blacksburg, VA 24061, USA
[d] Micro Materials Limited, Unit 3, Wrexham Technology Park, Wrexham, LL13 7YP, UK

ARTICLE INFO

Article history:
Received 4 January 2011
Received in revised form 9 February 2011
Accepted 12 February 2011
Available online 21 February 2011

Keywords:
Nanoindentation
Creep
Glass-ceramic
High-temperature

ABSTRACT

Mechanical properties of solid oxide fuel cell glass-ceramic seal material, G18, are studied at high temperatures. Samples of G18 are aged for either 4 h or 100 h, resulting in samples with different crystallinity. Reduced modulus, hardness, and time-dependent behavior are measured by nanoindentation. The nanoindentation is performed at room temperature, 550, 650, and 750 °C, using loading rates of 5 mN s^{-1} and 25 mN s^{-1}. Results show a decrease in reduced modulus with increasing temperature, with significant decrease above the glass transition temperature. Hardness generally decreases with increasing temperature, with a slight increase before Tg for the 4 h-aged sample. Dwell tests show that creep increases with increasing temperature, but decrease with further aging.

1. Introduction

Solid oxide fuel cells (SOFCs) have shown a high efficiency as an energy conversion device. In planar SOFCs, a hermetic seal is required to separate fuel and air sides of the electrodes. This seal must be able to withstand the thermal cycling experienced by the fuel cell, which operates at approximately 800 °C. Also, it is important that the joining temperature of the seal is above the operating temperature of the fuel cell it is intended for. One challenge SOFC industry is facing currently is sealing technology, which is usually broken or cracked after a short lifetime. Glass-ceramic materials are currently used as a candidate for SOFC sealant materials. Glass-ceramics maintain their mechanical properties at high temperatures, manufacturability, and low cost. The seal bonds several components in the cell (e.g. interconnect, electrodes, frames, etc.), therefore making it costly to replace. Seal materials must have long life spans due to their difficulty to repair [1–5].

Furthermore, a SOFC seal must not display significant creep at high temperatures to maintain the stack level geometric stability. By understanding the creep properties, the life of the seal may be predicted in terms of creep deformation. In the case of glass-ceramics, thermal and mechanical properties can be tailored by altering the degree of crystallinity. In this study, nanoindentation is performed on G18, a glass-ceramic seal developed by Pacific Northwest National Laboratory [3–8] to determine its temperature- and time-dependent viscoplastic properties. Nanoindentation has been used in other studies, especially for polymers, in characterizing creep properties [9–14]. The mechanical properties and creep behavior have previously been studied by nanoindentation at lower temperatures [15]. Also, the elastic modulus and creep behavior have been studied using dynamic resonance and relaxation tests, respectively [8]. Because G18 is a glass-ceramic designed for high temperature operation, it displays similar viscoplastic characteristics as polymers at high temperatures. High-temperature nanoindentation is used to establish relationships between mechanical properties and microstructure for the SOFC seal material. With better mechanical property–microstructure relationships, development of glass-ceramic seals could be more rapid and progressive. This is because altering the amount of crystallinity can easily change the mechanical properties. Nanoindentation of samples with different levels of crystallinity can show the effects of crystalline volume fraction.

G18 is a multi-phase glass-ceramic, which has an initial crystallinity after sintering and 4 h of aging at 750 °C is approximately 54%. The main crystalline phase is barium silicate. There are also small amounts of hexacelsian and barium orthosilicate after initial sintering and heat treatment. Initially the crystalline phases appear as needles, but after several hours of aging, phase boundaries blur. Beyond 100 h of aging, the hexacelsian and barium orthosilicate begin to disappear at the expense of developing monoclinic celsian. Crystallinity increases with aging and plateaus at 72%, while barium silicate remains the primary crystalline phase. Micrographs

* Corresponding author. Tel.: +1 404 385 2235; fax: +1 404 894 9140.
E-mail addresses: jmilhans@gatech.edu, jackie.milhans@gmail.com (J. Milhans).

0378-7753/$ – see front matter © 2011 Elsevier B.V. All rights reserved.
doi:10.1016/j.jpowsour.2011.02.033

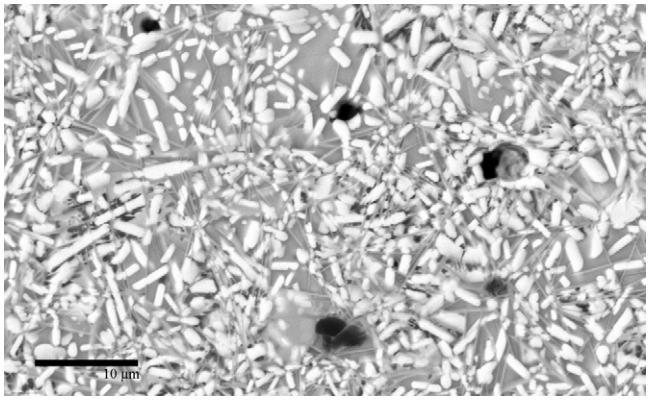

Fig. 1. SEM micrograph of G18 sintered at 800 °C and aged for 4 h.

of G18 aged 4 h and 1000 h are shown in Figs. 1 and 2, respectively. The brightest phase is the barium silicate phase. Darker grey needles observed in Fig. 1 are hexacelsian needles. The darkest phase is pores. It can be seen that the G18 aged for 1000 h is more porous and has a higher crystallinity than the G18 aged for 4 h.

In this study, nanoindentation is performed to measure the elastic modulus, hardness, and creep of G18. The tests are performed at 25, 550, 650, and 750 °C, using a c-BN, cubic boron nitride, tip. The glass transition temperature (Tg) for G18 is 620 °C. During nanocreep testing, the indenter is held at the maximum load for a certain period of time. This results in material creep following indentation, which is dependent on the load and holding time. The nanocreep tests help in understanding the creep behavior of G18.

Creep measurements will enable us to better understand the long-term effects of pressure on the seal at high temperatures. Nonlinear crystal viscoplasticity models will later be employed in order to predict long-term time-dependent behavior [2,6,16,17]. In this paper, we report the creep experiments and the data measured for G18.

2. Procedure

2.1. Materials and processing

Glass-ceramic G18 disks were pressed and sintered at 850 °C for 1 h. The samples were then aged at 750 °C for 4 h. A second sample of G18 was aged further for an additional 100 h at 800 °C. Longer aging results in higher crystallization of the sample. After aging for 100 h, crystallinity approaches saturation, and the samples will not age further during operation. The purpose of using sample aged for different times is to study the influence of crystallinity in the properties of the seal material. The samples were ground and polished for nanoindentation. Minimal sample damage occurs during grinding and polishing. Any damage would be revealed by steps in the loading portion of the indentation curve or a change in surface depth.

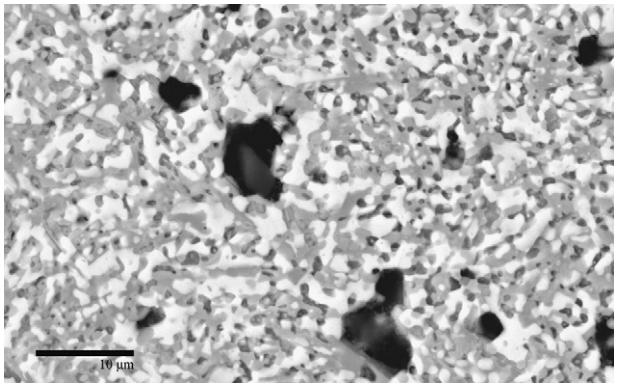

Fig. 2. SEM micrograph of G18 sintered at 800 °C and aged for 1000 h.

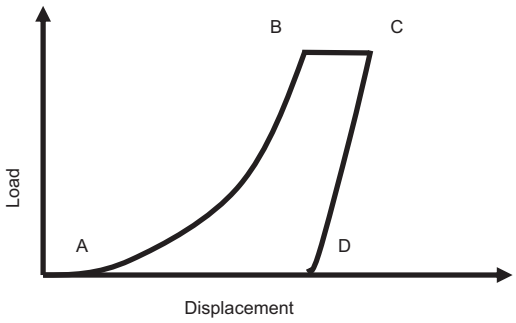

Fig. 3. Load–displacement curve of nanoindentation showing loading, load holding, and unloading.

2.2. Nanoindentation background

The modulus and hardness are calculated using the Oliver–Pharr method [18,19] from the load–displacement curves. A typical indentation curve is shown in Fig. 3, where from A to B is the loading portion of the curve, B to C shows a constant hold for the load, and C to D displays unloading. The elastic modulus and hardness are calculated using the unloading portion of the curve.

Several indentation parameters are needed to calculate the modulus and hardness using the Oliver–Pharr method. The indentation curve, seen in Fig. 4 can be described by the Oliver–Pharr method as [18]:

$$P = A(h - hf)^m \quad (1)$$

where P is load. A and m are material constants. Depth of the indentation, h, is acquired from the indentation, where h_c is the contact depth, h_s is the displacement at the perimeter of the indent. Total depth is defined by:

$$h = h_c + h_s \quad (2)$$

P_{max} represents the maximum load, which corresponds to the depth h_{max}. At this point, the stiffness is the initial unloading stiffness, S_{max}. These parameters are shown in Fig. 4.

The area of contact is calculated as a function of the contact depth, shown below for a Berkovich indenter tip [18]:

$$A_c = 3\sqrt{3h_c^2}\ \tan^2 65.3 = 24.5h_c^2 \quad (3)$$

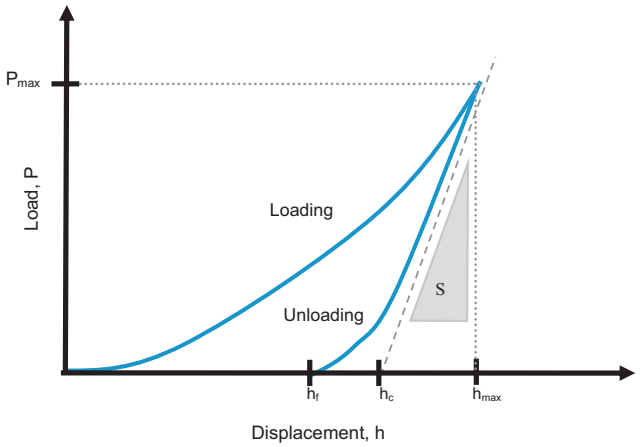

Fig. 4. Representation of load–displacement curve showing analysis parameters.

The stiffness is calculated according to the load, depth, contact area, and reduced modulus by the following relation [18]:

$$S = \frac{dp}{dh} = 2E_r \frac{\sqrt{A_c}}{\sqrt{\pi}} \tag{4}$$

The reduced modulus is given by [18]:

$$\frac{1}{E_r} = \frac{1-\nu_i^2}{E_i} + \frac{1-\nu_s^2}{E_s} \tag{5}$$

where ν is the Poisson's ratio, E is the elastic modulus, and i and s represent the indenter tip and specimen. In the following results, the indenter tip is assumed rigid, and the reduced modulus is taken to be the elastic modulus. Also, hardness was calculated, with the contact depth calculated at $h = h_{max}$, using the relationship [18]:

$$H = \frac{P_{max}}{24.5h_c^2} \tag{6}$$

2.3. Nanoindentation parameters

Samples were mounted to a high-temperature stage. Two sets of measurements were taken at 25, 550, 650, and 750 °C. The first set had a maximum load of 50, with a 5 mN s^{-1} loading rate; the second set had a maximum load of 120 mN with a 25 mN s^{-1} loading rate. Higher loading rates are more likely to cause viscoelastic deformation during the loading segment [2]. For each set of parameters, 5–10 indents were taken, spaced 30 μm apart. The reduced modulus and hardness were measured from the unloading curves. Creep measurements were taken using dwell periods of 120 s, held at maximum load. A c-BN indenter was used for all measurements. The results are considered to be global results, and not phase specific. This is due to the fact that the crystalline needles, generally having a width and length of 3 and 7 μm, are smaller than the approximate 10 μm indentation diameter. The nanoindentation was performed using a NanoTest platform from Micro Materials, Ltd., UK.

3. Results and discussion

3.1. Reduced modulus and hardness

The reduced modulus and hardness were measured by the unloading indentation curve. The results for loading rates 5 and 25 mN s^{-1} can be seen in Figs. 5–8. Results show that the material is strain rate sensitive at high temperatures, which is consistent with viscoplastic materials. The hardness and reduced modulus is higher at the lower loading rate.

At room temperature, the 4 h-aged sample has a higher modulus than the 100 h aged sample. This is consistent with findings from dynamic resonance results on 4 h-aged and 1000 h-aged G18 by Stephens et al. [8]. The dynamic resonance results for the 1000 h-aged sample do not display decreasing elastic modulus and hardness, where the nanoindentation results show that the elastic modulus and hardness for the 100 h-aged sample decreases with

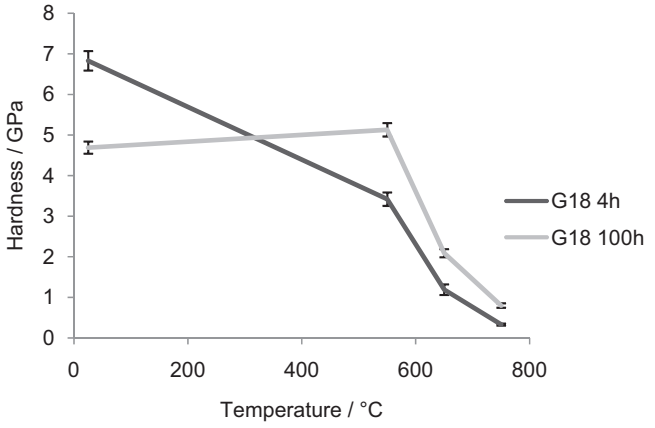

Fig. 6. Hardness of both samples with loading rate 25 mN s^{-1} with maximum load 120 mN.

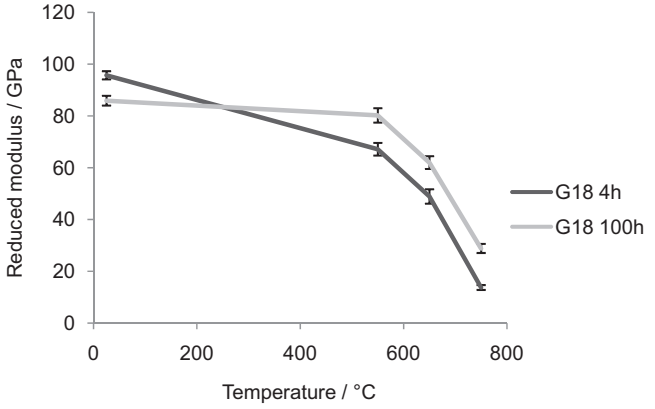

Fig. 7. Reduced modulus of both samples with loading rate 5 mN s^{-1} and maximum load 50 mN.

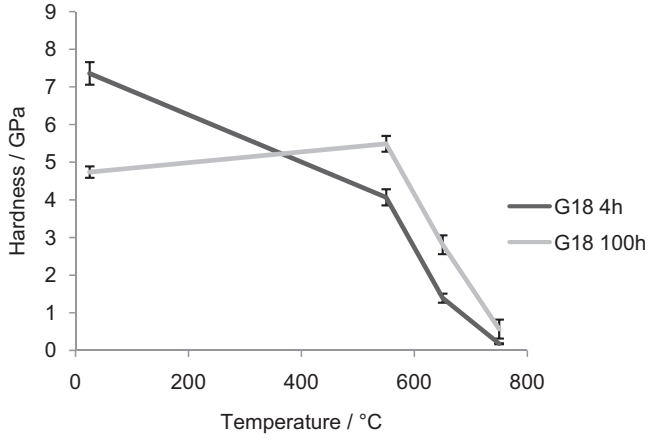

Fig. 5. Hardness of both samples with loading rate 5 mN s^{-1} with maximum load 50 mN.

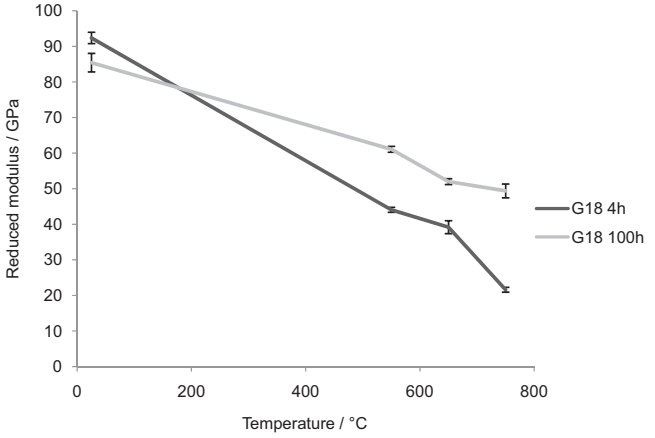

Fig. 8. Reduced modulus of both samples with loading rate 25 mN s^{-1} and maximum load 120 mN.

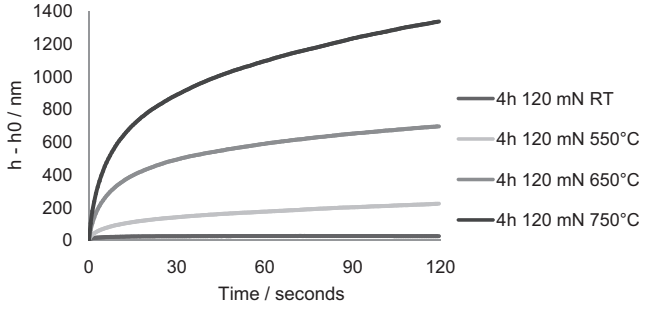

Fig. 9. Creep data for G18 aged for 4 h at maximum load 120 mN.

increasing temperature. This may be due to a lower amount of crystallinity in the 100 h-aged sample, in comparison to the 1000 h-aged sample tested in the dynamic resonance tests. The sample aged for 100 h shows a slight increase in hardness up to 550 °C. The sample aged for 4 h is significantly harder than G18 at room temperature, but decreases by half at 550 °C. This may be due to the higher amount of glassy phase in the lesser-aged sample. The low modulus for the G18 100 h-aged sample at room temperature is most likely due to cracking during cooling. As discussed earlier, further aged samples contain micro-voids in the glass phase, surrounding the crystalline phase. The micro-voids, combined with the brittle nature of the glass-ceramic at low temperature, may cause cracking when the material is cooled below Tg, 619 °C. Above 500 °C, results have shown an increase in modulus for the 100 h-aged sample, which is most likely due to self-healing of the material. The hardness of both samples drop rapidly above Tg and become more similar at 750 °C. Very similar values are obtained at both loading rates.

The 100 h-aged sample displays a small increase in reduced modulus up to 550 °C, while the 4 h-aged sample shows a drop of about 30% when measured at 50 mN and about 50% when measured at 120 mN. When measured at 50 mN, both samples show a similar decrease in modulus above 550 °C. When measured at 120 mN, both samples show a near linear reduction in modulus with increasing temperature. When measured at 120 mN the decrease rate in modulus is faster for 4 h G18. This is again probably due to the lower crystallinity of the 4 h-aged sample. The large difference between the 50 mN and 120 mN measurements is most likely due to cracking under the higher load.

3.2. Creep

Dwell periods of 120 s were performed at the maximum load of each indentation test. Typical to indentation creep tests, the results are shown as a function of change in depth, rather than strain. Creep results from the 120 mN maximum load tests are shown in Figs. 9 and 10, and results from the 50 mN maximum load tests are shown in Figs. 11 and 12. Results from the 50 mN maximum load tests displayed very similar results.

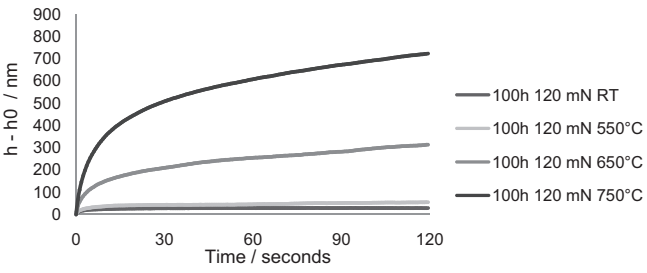

Fig. 10. Creep data for G18 aged for 100 h at maximum load 120 mN.

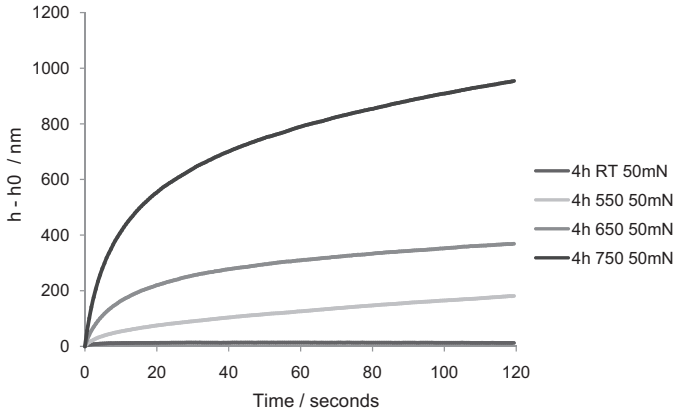

Fig. 11. Creep data for G18 aged for 4 h at maximum load 50 mN.

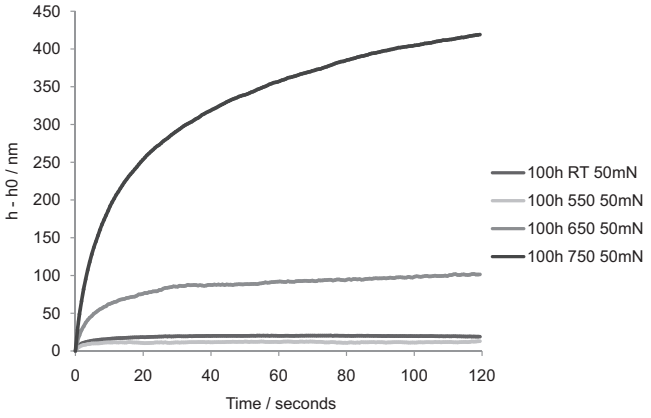

Fig. 12. Creep data for G18 aged for 100 h at maximum load 50 mN.

The data shows that creep become greater with increasing temperature and load. This is consistent with earlier findings by Stephens et al., using stress relaxation and short-term compression creep tests [8]. Above Tg, creep is significant. The 4 h-aged sample displays more creep than the 100 h aged sample. This was also expected, since the 100 h aged sample has a higher crystallinity than the 4 h-aged sample. The crystalline phases, due to their higher Tg, are most likely impeding flow of the glassy phase. Creep is consistent with earlier tests, showing the secondary creep, or steady-state, begins after a very short period of time, less than a minute [15]. Secondary creep occurs after primary creep, the rapid increase in strain after the load is applied. Secondary creep can be described as the constant deformation over time, which is due to work hardening.

4. Conclusions

The temperature dependent elastic modulus, hardness, and creep behavior of SOFC sealant ceramic-glass G18 with different crystallinity were studied under two different loading rates. The hardness of the 4 h-aged sample increased at 550 °C, then decreased with increasing temperature. The hardness of the 100 h aged sample decreased with increasing temperature. The reduced modulus of both samples decreased with increasing temperature, with a significant decrease above Tg. The discrepancies between the 50 mN and 120 mN maximum load data are most likely due to cracking that may have occurred under 120 mN. Dwell tests show that secondary creep begins after less than a minute. Creep increases as temperature increases, with large effects above Tg. Creep is also more significant when a large load is applied. Also, the 100 h aged

sample experienced less strain than the 4 h-aged sample, which is most likely due to the higher crystallinity in the sample.

Acknowledgements

The Pacific Northwest National Laboratory is operated by Battelle Memorial Institute for the United States Department of Energy under Contract DE-AC06-76RL01830. The work summarized in this report was funded as part of the Solid-State Energy Conversion Alliance (SECA) Core Technology Program by the U.S. Department of Energy's National Energy Technology Laboratory (NETL). Funding was additionally provided by the Boeing Fellowship.

References

[1] N. Lahl, L. Singheiser, K. Hilpert, Proc. Electrochem. Soc. SOFC-IV (1999) 1057–1066.
[2] S. Yang, Y. Zhang, K. Zeng, J. Appl. Phys. 95 (2004) 3655–3666.
[3] Z. Yang, K. Meinhardt, J. Stevenson, J. Electrochem. Soc. 150 (2003) A1095–A1101.
[4] Z. Yang, J. Stevenson, K. Meinhardt, Solid State Ionics 160 (2003) 213–225.
[5] K. Weil, J. Deibler, J. Hardy, D. Kim, G. Xia, L. Chick, C. Coyle, J. Mater. Eng. Perform. 13 (2004) 316–326.
[6] W. Liu, X. Sun, M. Khaleel, J. Power Sources 185 (2008) 1193–1200.
[7] Z. Yang, K. Weil, D. Paxton, J. Stevenson, J. Electrochem. Soc. 150 (2003) A1188–A1201.
[8] E. Stephens, J. Vetrano, B. Koeppel, Y. Chou, X. Sun, M. Khaleel, J. Power Sources 193 (2009) 625–631.
[9] H. Shang, T. Rouxel, J. Am. Ceram. Soc. 88 (2005) 2625–2628.
[10] H. Shang, T. Rouxel, M. Buckley, C. Bernard, J. Mater. Res. 21 (2006) 632–638.
[11] B. Briscoe, L. Fiori, E. Pelillo, J. Phys. D: Appl. Phys. 31 (1998) 2395–2405.
[12] B. Briscoe, K. Sebastian, M. Adams, J. Phys. D: Appl. Phys. 27 (1994) 1156–1162.
[13] B. Beake, G. Bell, W. Brostow, W. Chonkaew, Polym. Int. 56 (2007) 773–778.
[14] B. Beake, J. Smith, Philos. Mag. A 82 (2002) 2179–2186.
[15] J. Milhans, M. Khaleel, X. Sun, M. Tehrani, M. Al-Haik, H. Garmestani, J. Power Sources 195 (2010) 3631–3635.
[16] M. Vanlandingham, J. Villarrubia, W. Guthrie, G. Meyers, Macromol. Symp. 167 (2001) 15–43.
[17] M. Oyen, R. Cook, J. Mater. Res. 18 (2003) 139–150.
[18] W. Oliver, G. Pharr, J. Mater. Res. 7 (1992) 1564–1583.
[19] G. Pharr, W. Oliver, F. Brotzen, J. Mater. Res. 7 (1992) 613–617.